Ramakrishna Mission Residential College (Autonomous)
Kolkata 700103, WB, India

Collaborative research in coordination chemistry of organic radicals

Number 2

Institute 1: Ramakrishna Mission Residential College (Autonomous)

Concerned Faculty: Dr. Prasanta Ghosh, Dept of Chemistry

&

Institute 2: **Max-Planck-Institut für Chemische Energiekonversion**

Stiftstrasse 34 - 36 / D - 45470 Mülheim an der Ruhr

Concerned Scientist: Dr Thomas Weyhermüller

Period of Investigation: 01-09-2014 to 01-03-2015

Project: Transition metal complexes of α-diimine ligands: Syntheses, structures and photoluminescence

Output: The result was published in a journal of international repute

Publication: Mononuclear zinc(II), cadmium(II), cobalt(III) and di-nuclear nickel(II) complexes of a 14-pi electron diimine ligand: Syntheses, structures, photoluminescence and DFT investigations

Satyabrata Chaudhuri, Suman Kundu, Manas Kumar Biswas, Thomas Weyhermüller and Prasanta Ghosh*

Inorg.Chim. Acta, 2015, *430*, 199-207

Dr. Prasanta Ghosh

Dr Thomas Weyhermüller

Inorganica Chimica Acta 430 (2015) 199–207

Contents lists available at ScienceDirect

Inorganica Chimica Acta

journal homepage: www.elsevier.com/locate/ica

Mononuclear zinc(II), cadmium(II), cobalt(III) and di-nuclear nickel(II) complexes of a 14pi electron diimine ligand: Syntheses, structures, photoluminescence and DFT investigations

Satyabrata Chaudhuri [a], Suman Kundu [a], Manas Kumar Biswas [a], Thomas Weyhermüller [b], Prasanta Ghosh [a,*]

[a] Department of Chemistry, R. K. Mission Residential College, Narendrapur, Kolkata 700103, India
[b] Max-Planck-Institut für Chemische Energiekonversion, Stiftstrasse 34-36, D-45470 Mülheiman der Ruhr, Germany

ARTICLE INFO

Article history:
Received 14 October 2014
Received in revised form 9 January 2015
Accepted 18 February 2015
Available online 14 March 2015

Keywords:
Coordination complexes of 14π electron diimine ligand
Fluorescence spectra
DFT calculations

ABSTRACT

Three types of fluorescent coordination complexes of an unsymmetrical diimine ligand (L_{NNOH}) with conjugated 14π electrons (14πe) are reported [L_{NNOH} = (*E*)-2-((phenyl(pyridin-2-yl)methylene) amino) phenol]. The complexes are: $[M(L_{\bar{N}NO})X]$ [M = Zn, X = Cl, **1**; M = Zn, X = Br, **2**; M = Cd, X = Cl, **3**], $[Co(L_{\bar{N}NO})_2]Cl$, [**4**]Cl and $[Ni_2(L_{NNOH})_2(L_{\bar{N}NO})_2]Cl_2$, [**5**]$Cl_2$. The complexes were substantiated by elemental analyses, IR, ^1H NMR, mass and UV–Vis spectra including the single crystal X-ray structure determinations of [**4**]Cl·H_2O and [**5**]Cl_2·$2H_2O$. Complexes **1–3** and [**4**]Cl are brightly fluorescent in fluid solutions (CH_2Cl_2: **1**, λ_{ex} = 475, 507 nm, λ_{em} = 520, 551 nm, Φ = 0.037, τ_{av} = 2.6 ns; **2**, λ_{ex} = 474, 507 nm, λ_{em} = 519, 552 nm, Φ = 0.027, τ_{av} = 2.4 ns; **3**, λ_{ex} = 474, 507 nm, λ_{em} = 518, 551 nm, Φ = 0.01, τ_{av} = 2.0 ns; [**4**]Cl, λ_{ex} = 472, 505 nm, λ_{em} = 518, 551, 601 nm, Φ = 0.06, τ_{av} = 3.9 ns) while [**5**]Cl_2 is weakly emissive (CH_2Cl_2: λ_{ex} = 472, 506 nm, λ_{em} = 520, 557, 595 nm, Φ = 0.002, τ_{av} = 1.9 ns). Variable temperature magnetic measurement and Mulliken atomic spin densities obtained from unrestricted density functional theory (DFT) calculation on $[\mathbf{5}]^{2+}$ cation, are consistent with the existence of weakly interactive (J = +2.318) two Ni(II) ions. Time dependent (TD) DFT calculations on **1** and $[\mathbf{4}]^+$ authenticated the intra-ligand $\pi_{phenolato} \rightarrow \pi^*_{diimine}$ transitions for **1–3** and both intra- and inter-ligand $\pi_{phenolato} \rightarrow \pi^*_{diimine}$ transitions for [**4**]Cl as the origins of the emissive excitations.

1. Introduction

Coordination complexes of α-diimines are photofunctional [1]. Recently, we disclosed that the photoluminescence property of the α-diimine complexes depends on the number of π electron present in the conjugated diimine system [2]. It is reported that the unsymmetrical diimines with 14π electrons (14πe) of type L_R^{ϕ} at $\phi = 0°$ as depicted in panel (a) of Chart 1 are π-isoelectronic with anthracene and the crystals of $[M(L_R^{\phi})X_2]$ (M = Zn, Cd; X = Cl, Br) complexes emit at 298 K [2a]. Because of the atropisomerism [2a] even after coordination to a metal ion, L_R^{ϕ} behaves more like a (8π + 6π) electrons system at $\phi \neq 0°$ in solution as shown in panel (b) of Chart 1 and the fluid solutions of $[M(L_R^{\psi})X_2]$ complexes are non-luminescent. However in frozen glasses they are fluorescent. Moreover, in crystals due to π–π stacking that results $\pi^*_{diimine}$ delocalization over the layers, emission maxima of $[M(L_R^{\phi})X_2]$ are red shifted compared to those in frozen glasses.

In this project, we have been successful to restrict the atropisomerism of the pendent aromatic ring (with the 6πe) introducing the OH substituent at the ortho position to the imine function of L_H^{ϕ} that coordinates the metal ion as a tridentate NNO-chelate (panel (c) of Chart 1) preserving the orientation with $\phi = 0°$. The tri-dentate NNO-chelating agent is abbreviated as L_{NNOH} which upon coordination to a metal ion sustains as a delocalized 14πe chromophore even in solution [L_{NNOH} = (*E*)-2-((phenyl(pyridin-2-yl) methylene)amino)phenol]. The notable effect is that L_{NNOH} affords three types of fluorescent complexes with zinc(II), cadmium(II), cobalt(III) and nickel(II) ions. With zinc(II) and cadmium(II) ions it yields mono-nuclear $[M(L_{\bar{N}NO})X]$ [M = Zn, X = Cl, **1**; M = Zn, X = Br, **2**; M = Cd, X = Cl, **3**] complexes. The reaction of L_{NNOH} with anhydrous $CoCl_2$ generates a mono-nuclear bis-$L_{\bar{N}NO}$ complex of type $[Co(L_{\bar{N}NO})_2]Cl$, [**4**]Cl. With nickel(II) ion, it produces an unusual paramagnetic phenoxide bridged binuclear complex of type $[Ni_2(L_{NNOH})_2(L_{\bar{N}NO})_2]Cl_2$, [**5**]$Cl_2$. The coordination features of **1–3**,

* Corresponding author. Tel.: +91 33 2428 7347; fax: +91 33 2477 3597.
E-mail address: ghosh@pghosh.in (P. Ghosh).

http://dx.doi.org/10.1016/j.ica.2015.02.032
0020-1693/

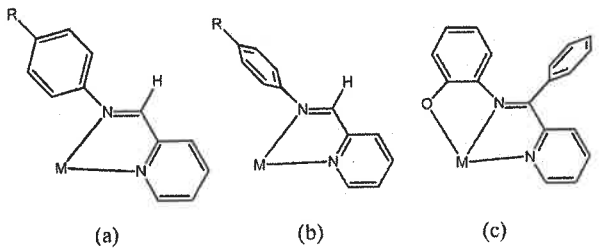

Chart 1. (a) $M(L_R^{\psi})$ unit with $\phi = 0$, $14\pi e$ system (b) $M(L_R^{\psi})$ unit with $\phi = 90$, $(8\pi + 6\pi)e$ system and (c) $M(L_{\bar{N}NO})$ unit with $\phi = 0$, $14\pi e$ system.

[4]Cl and **[5]Cl_2** are shown in Chart 2. On the contrary to the $[M(L_R^{\phi})X_2]$ complexes, all these three types of complexes of L_{NNOH} are fluorescent in fluid solutions at 298 K.

In this article, syntheses and spectra of the complexes including the single crystal X-ray structure of **[4]Cl**·H_2O are reported. Density functional theory (DFT) and the time dependent (TD) DFT calculations established the origins of excitations of the complexes. The constituents of the photoactive orbitals of these three types of fluorescent complexes are analyzed. The atropisomerism restricted fluorescence of the complexes of L_{NNOH}, that does not occur in heterocyclic symmetrical rigid diimines, like 2,2′-bipyridine or 1,10-phenanthroline incorporating 12π electrons only, is a worth investigation in searching photoactive materials in the vast coordination chemistry.

2. Experimental

2.1. Materials and physical measurements

Reagents or analytical grade materials were obtained from Sigma–Aldrich and used without further purification. Spectroscopic grade solvents were used for spectroscopic measurements. After evaporating H_2O and MeOH solvents of the sample under high vacuum, elemental analyses and spectral measurements were performed. The C, H and N content of the compounds were obtained from a *Perkin-Elmer 2400 series II* elemental analyzer. Infrared spectra of the samples were recorded from 4000 to 400 cm^{-1} with the KBr pellet at 298 K on a *Perkin-Elmer Spectrum RX 1*, FT-IR Spectrophotometer. ^1H NMR spectrum in $CDCl_3$ solvents was carried out on a *Bruker DPX-300 MHz spectrometer* with tetramethylsilane (TMS) as an internal reference. ESI mass spectra were recorded on a micro mass *Q-TOF mass spectrometer*. Electronic absorption spectra in solutions at 298 K were carried out on a *Perkin-Elmer Lambda 25* spectrophotometer in the range of 1100–200 nm. Variable temperature (3–300 K) magnetization data were recorded in a 1 *T* magnetic field on a *SQUID magnetometer* (MPMS Quantum Design). The experimental magnetic susceptibility data were corrected for underlying diamagnetism using tabulated Pascal's constants.

2.2. Syntheses

2.2.1. $[Zn(L_{\bar{N}NO})Cl]$ (1)

To 2-benzoyl pyridine (366 mg, 2 mmol) and 2-aminophenol (218 mg, 2 mmol) in a round bottom flask, methanol (25 mL) was added and the resulting solution was heated to reflux for 1.5 h. The reaction mixture was cooled at 298 K. To this solution, a solution of anhydrous zinc chloride (275 mg, 2 mmol) in methanol (10 mL) was added. The reaction mixture was allowed to evaporate slowly in air. After 3–4 days, red crystalline compound separated out, which was collected upon filtration and dried in air Yield: 523 mg (~70% with respect to zinc). Mass spectrum (ESI, positive ion, CH_3OH); *m/z*: 338.9 for $[1\text{-Cl}]^+$. *Anal.* Calc. for $C_{18}H_{13}N_2OZnCl$: C, 57.78; H, 3.50; N, 7.49; Found: C, 57.42; H, 3.39; N, 7.25%. ^1H NMR ($CDCl_3$, 300 MHz, 300 K): δ 8.95 (d, 1H), 8.12 (d, 1H), 8.02 (d, 2H), 7.65 (m, 4H), 7.54 (t, 2H), 7.41–7.34 (m, 3H) ppm. IR (KBr disk): ν 3446 (vs), 1583 (s), 1458 (m), 1270 (vs), 1141 (m), 765 (s), 710 (m) cm^{-1}.

2.2.2. $[Zn(L_{\bar{N}NO})Br]$ (2)

To 2-benzoyl pyridine (366 mg, 2 mmol) and 2-aminophenol (218 mg, 2 mmol) in a round bottom flask, methanol (25 mL) was added and the resulting solution was heated to reflux for 1.5 h. The reaction mixture was cooled at 298 K. To this solution, a solution of anhydrous zinc bromide (400 mg, 2 mmol) in methanol (15 mL) was added. The reaction mixture was allowed to evaporate slowly in air. After 3–4 days, red crystalline compound separated out, which was collected upon filtration and dried in air. Yield: 544 mg (~65% with respect to zinc). Mass spectrum (ESI, positive ion, CH_3OH); *m/z*: 338.69 for $[2\text{-Br}]^+$. *Anal.* Calc. for $C_{18}H_{13}N_2OZnBr$: C, 51.65; H, 3.13; N, 6.69; Found: C, 51.55; H, 3.01; N, 6.47%. ^1H NMR ($CDCl_3$, 300 MHz, 300 K): δ 8.85 (d, 1H), 8.10 (d, 1H), 8.05 (d, 2H), 7.67 (m, 4H), 7.52 (t, 2H), 7.38 (m, 3H) ppm. IR (KBr disk): ν 3446 (vs), 1684 (s), 1653 (vs), 1583 (vs), 1559 (vs), 1458 (vs), 1267 (vs), 1141 (m), 764 (s), 710 (m) cm^{-1}.

2.2.3. $[Cd(L_{\bar{N}NO})Cl]$ (3)

To 2-benzoyl pyridine (366 mg, 2 mmol) and 2-aminophenol (218 mg, 2 mmol) in a round bottom flask, methanol (25 mL) was added and the resulting solution was heated to reflux gently for 1.5 h. The reaction mixture was cooled at 298 K. To this solution, a solution of anhydrous cadmium chloride (366 mg, 2 mmol) in methanol (15 mL) was added. The reaction mixture was allowed to evaporate slowly in air. After 3–4 days, orange crystalline compound separated out, which were collected upon filtration and dried in air. Yield: 522 mg (~62% with respect to cadmium).

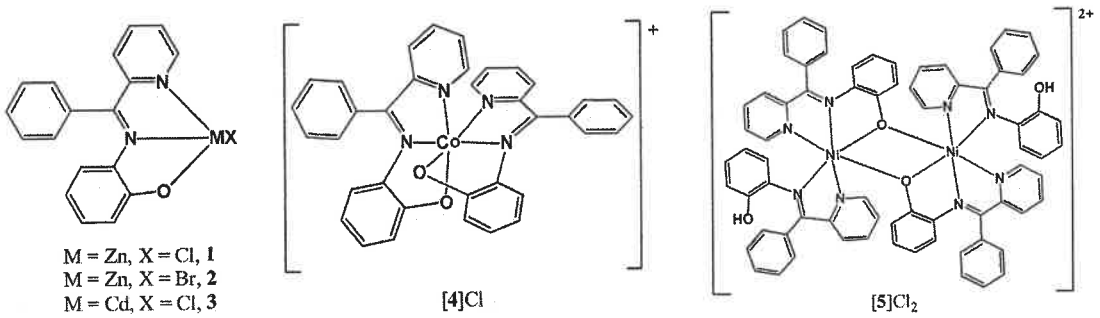

Chart 2. $[M(L_{\bar{N}NO})X]$, $[Co(L_{\bar{N}NO})_2]Cl$, and $[Ni_2(L_{NNOH})_2(L_{\bar{N}NO})_2]Cl_2$ complexes.

Mass spectrum (ESI, positive ion, CH_3OH); *m/z*: 385.61 for **[3-Cl]**$^+$. *Anal.* Calc. for $C_{18}H_{13}N_2OCdCl$: C, 51.34; H, 3.11; N, 6.65; Found: C, 51.27; H, 3.01; N, 6.53%. ^{1}H NMR ($CDCl_3$, 300 MHz, 300 K): δ 9.39 (d, 1H), 8.75 (d, 1H), 8.05 (d, 1H), 7.75 (t, 1H), 7.59 (d, 2H), 7.49 (t, 2H), 7.06 (t, 2H), 6.70 (t, 1H), 6.42 (t, 1H), 6.11 (d, 1H) ppm. IR (KBr disk): *v* 3232 (vs), 1590 (s), 1488 (s), 1321 (s), 1263 (s), 1017 (m), 979 (m), 763 (s), 702 (s) cm^{-1}.

2.2.4. $[Co(L_{\bar{N}NO})_2]Cl{\cdot}H_2O$ ([4]Cl·H_2O)

To 2-benzoyl pyridine (366 mg, 2 mmol) and 2-aminophenol (218 mg, 2 mmol) in a round bottom flask, methanol (25 mL) was added and the resulting solution was heated to reflux gently for 1.5 h. The reaction mixture was cooled at 298 K. To this solution, a solution of anhydrous cobalt(II) chloride (258 mg, 2 mmol) in methanol (15 mL) was added. The resulting dark red solution was allowed to evaporate slowly in the air. After 2–3 days, red crystals of **[4]**Cl·H_2O separated out, which were collected upon filtration and dried in air. Yield: 704.5 mg (~55% with respect to cobalt). Mass spectrum (ESI, positive ion, CH_3OH); *m/z*: 605.01 for **[4]**$^+$. *Anal.* Calc. for $C_{36}H_{26}ClCoN_4O_2$: C, 67.45; H, 4.09; N, 8.74; Found: C, 67.36; H, 4.01; N, 8.53%. ^{1}H NMR ($CDCl_3$, 300 MHz, 300 K): δ 8.35 (d, 2H), 8.14–8.06 (br, 5H), 7.82 (d, 1H), 7.33 (m, 4H), 7.08–6.90 (m, 7H), 6.76 (d, 2H), 6.68 (d, 2H), 6.53 (d, 1H), 6.33 (t, 2H) ppm. IR (KBr disk): *v* 3422 (br), 1631 (s), 1595 (vs), 1382 (m), 1350 (m), 1113 (m), 749 (m) cm^{-1}.

2.2.5. $[Ni_2(L_{NNOH})_2(L_{\bar{N}NO})_2]Cl_2{\cdot}2H_2O$ ([5]$Cl_2{\cdot}2H_2O$)

To a MeOH (30 mL) solution of 2-benzoylpyridine (366 mg, 2 mmol), 2-aminophenol (436 mg, 4 mmol) was added and resulting solution was refluxed for 1.5 h. The solution was cooled to room temperature and filtered. To this resulting solution anhydrous $NiCl_2$ (260 mg, 2 mmol) was added. The resulting dark brown solution was allowed to evaporate slowly in air. Within 2–3 days, brown crystals of **[5]**$Cl_2{\cdot}2H_2O$ separated out, which were collected upon filtration and dried in air. Yield: 558 mg (~48% with respect to nickel). Mass spectrum (ESI, positive ion, CH_3OH); *m/z*: 605.10 for **[5/2]**$^+$. *Anal.* Calc. for $C_{68}H_{54}N_8O_4Ni_2$: C, 74.21; H, 4.94; N, 10.18; Found: C, 74.19; H, 4.86; N, 10.11%. IR (KBr disk): *v* 3854 (s), 3751 (s), 3650 (s), 3398 (s), 1593 (vs), 1458 (vs), 1270 (vs), 745 (vs), 701 (s) cm^{-1}.

2.3. Structure determination

Single crystals of **[4]**Cl·H_2O and **[5]**$Cl_2{\cdot}2H_2O$ were picked up with nylon loops and mounted on a *Bruker APEX-II CCD* diffractometer equipped with a Mo-target rotating-anode X-ray source and a graphite monochromator (Mo Kα, λ = 0.71073 Å). **[4]**Cl·H_2O was measured at 100 K and **[5]**$Cl_2{\cdot}2H_2O$ was measured at 296 K. Final cell constants were obtained from least squares fits of all measured reflections. Intensity data were corrected for absorption using intensities of redundant reflections. The structures were readily solved by direct methods and subsequent difference Fourier techniques. The crystallographic data of **[4]**Cl·H_2O are listed in Table 1. The crystals of **[5]**$Cl_2{\cdot}2H_2O$ are weakly diffracting and several attempts to have better data set failed. No crystal data and bond parameters of it were reported here. The Siemens SHELXS97 [3] software package was used for solution and SHELXL97 [3] was used for the refinement. All non-hydrogen atoms were refined anisotropically. Hydrogen atoms were placed at the calculated positions and refined as riding atoms with isotropic displacement parameters.

2.4. Density functional theory (DFT) calculations

All calculations reported in this article were done with the GAUSSIAN 03W [4] program package supported by GAUSSVIEW 4.1. The DFT [5] and TD DFT [6] calculations were performed at the level of Becke three parameter hybrid functional with the non-local correlation functional of Lee-Yang-Parr (B3LYP) [7]. Gas-phase geometries of **1**, **[4]**$^+$ and **[5]**$^{2+}$ were optimized using Pulay's Direct Inversion [8] in the Iterative Subspace (DIIS), 'tight' convergent SCF procedure [9] ignoring symmetry. In all calculation, a LANL2DZ basis set [10], along with the corresponding effective core potential (ECP) was used for zinc, cobalt and nickel metal atoms. Basis set 6-31G [11] was used for H atoms. For non-hydrogen atoms first polarization functions were added. Basis set 6-31G (d, p) [12] for C, N, O and Cl atoms are employed for the calculation. The percentage contribution of metal, chloride and ligands to the frontier orbitals of **1** and **[4]**$^+$, were calculated using GAUSSSUM program package [13]. The 60 lowest singlet excitation energies on the optimized geometry of **1** and **[4]**$^+$ in CH_2Cl_2 were calculated by TD DFT method [14] using conductor-like polarizable continuum model (CPCM).

Table 1
Crystallographic data for **[4]**Cl·H_2O.

CCDC	943148
Formula	$C_{36}H_{28}ClCoN_4O_3$
F_w	659.00
Crystal color/system	brown/monoclinic
Space group	*P*21/*c*
a (Å)	15.965(5)
b (Å)	11.228(2)
c (Å)	16.998(4)
β (°)	96.04(2)
V (Å^3)	3030.1(13)
Z	4
T (K)	100(2)
ρ_c (g cm^{-3})	1.445
$2\theta_{max}$	65.00
Unique reflections	143382
Reflections	10320
λ (Å)/μ (mm^{-1})	0.71073/0.699
F(000)	1360
R_1[a] [$I > 2\sigma(I)$]	0.0660
GOF[b]	1.230
R_1[a] (all data)	0.0877
wR_2[c] [$I > 2\sigma(I)$]	0.1419
Parameters/restr.	412/2
Residual density (e Å^{-3})	1.814/−0.902

Observation criterion: $I > 2\sigma(I)$. where $w = 1/[\sigma^2(F_o^2) + (aP)^2 + bP]$, $P = (F_o^2 + 2F_c^2)/3$.
[a] $R_1 = \Sigma||F_o| - |F_c||/\Sigma|F_o|$.
[b] GOF = $\{\Sigma[w(F_o^2 - F_c^2)^2]/(n-p)\}^{1/2}$.
[c] $wR_2 = \{\Sigma[w(F_o^2 - F_c^2)^2]/\Sigma[w(F_o^2)^2]\}^{1/2}$.

2.5. Recording of excitation and emission spectra and lifetimes measurements

Excitation and emission spectra were recorded using quartz sample tube on *Perkin Elmer LS 55* luminescence spectrophotometer. Fluorescence quantum yield (ϕ_D) was determined in each case by comparing the corrected emission spectrum of the samples with that of anthracene in MeOH (ϕ_D = 0.20) and CH_2Cl_2 (ϕ_D = 0.30) using the Eq. (1) considering the total area under the emission curve [15].

$$Q = Q_R \frac{F}{F_R} \frac{OD_R}{OD} \frac{n^2}{n_R^2} \quad (1)$$

where *Q* is the quantum yield of the compounds, *F* is the integrated fluorescence intensity (area under the emission curve), *OD* is the optical density, and *n* is the refractive index of the medium. It is assumed that the reference and the unknown samples are excited at the same wavelength. The subscript *R* refers to the reference fluorophore (anthracene in this case) of known quantum yield. The standard quantum yield value thus obtained is used for the calculation of quantum yields of the systems under various conditions.

Singlet state lifetimes were measured by a Time Master Fluorimeter from Photon Technology International (PTI), USA. The system consists of a pulsed laser driver of a PDL series *i.e.*, PDL-800-B (from Pico-Quant, Germany) with interchangeable sub-nanosecond pulsed LEDs and pico-diode lasers (PicoQuant, Germany) with a TCSPC set-up (PTI, USA). The software Felix 32 controls all acquisition modes and data analyses of the Time Master system [16].

The lifetimes of all the complexes were measured by using TCSPC from PTI, USA using a diode laser LDH-470 (pulse width ~200 ps) (from Pico Quant, Germany) at a repetition frequency 10 MHz driven by a PDL 800-B driver, Pico-Quant, Germany. Instrument response functions (IRF) were measured at the respective excitation wavelength using slits with a band pass of ~1–3 nm using Ludox as the scatterer. Intensity decay curves were fitted as a sum of exponential terms:

$$F(t) = \sum \alpha_i \exp^{-t/\tau_i} \quad (2)$$

The decay parameters were recovered using a non-linear iterative fitting procedure based on the Marquardt algorithm. A deconvolution technique was used to determine the lifetime with the time resolution is 100 ps with diode lasers. The quality of fit has been assessed over the entire decay, including the rising edge, and tested with a plot of weighted residuals and other statistical parameters *e.g.*, the reduced χ^2 ratio and the Durbin–Watson (DW) parameters [16].

3. Results and discussion

3.1. Syntheses and characterization

Free L_{NNOH} ligand was not successfully isolated. The condensation between 2-benzoyl pyridine and 2-aminophenol only takes place in presence of a Lewis acid. In this work, metal salts were used as Lewis acids for the condensation reaction that afforded coordination complexes in situ. Using this procedure, we succeeded in isolating three types of coordination complexes of L_{NNOH} with zinc(II), cadmium(II), cobalt(III) and nickel(II) as illustrated in Chart 2. All the complexes were synthesized in high yields by stoichiometric reactions of 2-benzoyl pyridine, 2-aminophenol and the corresponding metal dihalides. ZnX_2 and CdX_2 salts afford mono-nuclear complexes of type $[M(L_{\bar{N}NO})X]$ (M = Zn, X = Cl, **1**; M = Zn, X = Br, **2**; M = Cd, X = Cl, **3**) while $CoCl_2$ affords a cobalt(III) complex, *mer*-$[Co(L_{\bar{N}NO})_2]Cl$, **[4]**Cl. The coordination feature of L_{NNOH} toward nickel(II) ion is different furnishing a dinuclear complex of type $[Ni_2(L_{NNOH})_2(L_{\bar{N}NO})_2]Cl_2$ **[5]**Cl_2. In **[5]**$Cl_2{\cdot}2H_2O$ two monoanionic $L_{\bar{N}NO}$ ligand bridges the metal ion by phenoxide ion. The remaining two ligands coordinate as neutral bi-dentate diimine ligands (L_{NNOH}) with the pendent phenolic-OH functions. In solution, **[5]**$Cl_2{\cdot}2H_2O$ decomposes as observed in mass spectra, 937.23 due to $[Ni_2(L_{NNO})_3]$, 607.16 due to $Ni(L_{NNO})_2$. The O–H stretching vibration of $[5]^{2+}$ di-cation resonates at 3392 cm^{-1}. The $\nu_{C=N}$ stretching frequencies of the complexes span the range 1590–1600 cm^{-1}. The ^1H NMR data of all the diamagnetic complexes in $CDCl_3$ solvent are assigned and are listed in the experimental section.

The UV–Vis absorption spectra of the complexes were recorded in MeOH and CH_2Cl_2 solvents at 298 K. Spectral data are summarised in Table 2 and the spectra are shown in Figs. 1 and S1 (S refers to Supplementary Material). The absorption spectral features of **1** and **2** are similar. The lower energy absorption maximum of **3** is blue shifted in CH_2Cl_2. The absorption maxima of **[4]**Cl in MeOH and CH_2Cl_2 are 435 and 448 nm. The absorption spectral features of **[5]**Cl_2 are comparable to those of **[4]**Cl complex. The origins of the UV–Vis absorption spectra of these complexes were elucidated by time dependent density functional theory (TD DFT) calculations (*vide infra*). All the complexes are diamagnetic except **[5]**Cl_2. The variable temperature magnetic moment of **[5]**Cl_2 is shown in Fig. 2. The measurement confirms the existence of two Ni(II) ions with J = +2.318 in **[5]**Cl_2.

Table 2
Electronic absorption spectral data of **1–3**, **[4]**Cl and **[5]**Cl_2 in CH_3OH and CH_2Cl_2 at 298 K.

Complexes	Solvent	λ_{max}, nm (ε, 10^4 M^{-1} cm^{-1})
1	MeOH	463(1.99), 328(1.84), 282(1.76), 233(3.34), 206(6.53)
	CH_2Cl_2	507(1.44), 475(1.23), 447(0.79), 355(0.38), 265(1.78)
2	MeOH	462(1.06), 330(0.95), 283(0.89), 232(1.74), 205(3.98)
	CH_2Cl_2	504(0.32), 437(0.70), 332(0.67), 276(1.16)
3	MeOH	460(0.90), 328(0.81), 277(1.39), 235(2.25), 206(4.76)
	CH_2Cl_2	393(0.61), 359(0.57), 272(2.37)
[4]Cl	MeOH	435(0.75), 273 (1.60), 226 (5.50)
	CH_2Cl_2	448(0.64), 353(1.31), 334(1.67), 315(1.85), 274(9.26)
[5]Cl_2	MeOH	484(2.30), 444(1.75), 323(2.87), 235(5.39), 206(9.99)
	CH_2Cl_2	431(1.77), 331(2.53), 273(5.95)

3.2. Molecular geometries

We failed to grow suitable single crystals of **1–3** for X-ray diffraction study. However, the molecular geometries of $[4]^+$ and $[5]^{2+}$ were confirmed by the single crystal X-ray structure determinations of **[4]**Cl·H_2O and **[5]**$Cl_2{\cdot}2H_2O$. **[4]**Cl crystallizes in $P2_1/c$ space group. The molecular structure with the atom labelling scheme is shown in Fig. 3. The relevant bond parameters are summarized in Table 3. L_{NNOH} is a tri-dentate ligand with the three different types of donor sites. In **[4]**Cl, two imine N atoms lie on the trans sites and the molecule is devoid of any kind of plane of symmetry. The CoN_4O_2 octahedron is distorted. The three trans angles are 170.76(9), 174.95(10) and 171.20(9)°. Each $L_{\bar{N}NO}$ ligand is

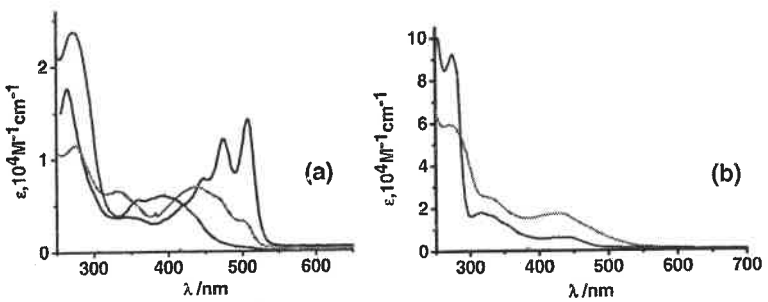

Fig. 1. UV–Vis absorption spectra of (a) **1** (black), **2** (red) and **3** (blue); (b) **[4]**Cl (green) and **[5]**Cl_2 (magenta) in CH_2Cl_2 298 K. (For interpretation of the references to color in this figure legend, the reader is referred to the web version of this article).

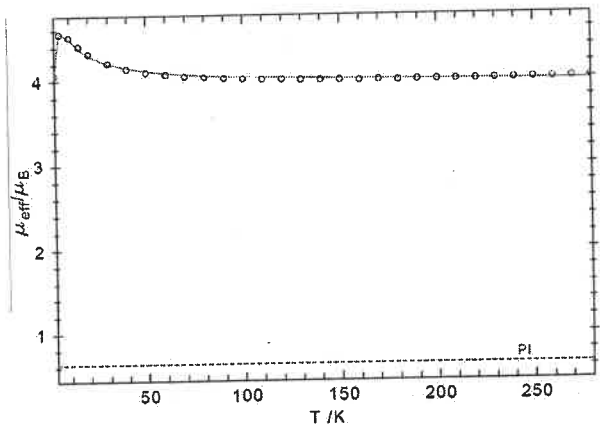

Fig. 2. Temperature-dependence of the magnetic moment, μ_{eff}/μ_B, of powdered sample of [5]Cl_2. The circles represent the experimental data, whereas the solid lines represent simulations.

planar and the pendent phenyl plane is perpendicular to this plane. The Co–$O_{phenolato}$, Co–$N_{pyridine}$ and Co–N_{imine} are comparatively shorter and are consistent with the presence of Co^{III} ion in $[4]^+$ cation. The Co^{III}–$O_{phenolato}$ distances are 1.887(2) and 1.884(2) Å. The Co^{III}–$N_{pyridine}$ lengths are 1.933(2) and 1.916(2) Å while the Co^{III}–N_{imine} distances are 1.888(2) and 1.884(2) Å.

[5]Cl_2·2H_2O crystallizes in the space group *C2/c*. Anion Cl^- and H_2O molecules in crystals are disordered and display inter-water molecular H-bonding (O7–O8 = 2.562 Å) and hydrogen bonding with non-coordinated phenolic-OH functions (O2–OH_2 = 2.755 Å; O4–OH_2 = 2.765 Å). Gross molecular geometry of the di-cation, $[5]^{2+}$ excluding the Cl^- ions and H_2O molecules is shown in Fig. 4. The X-ray structure unambiguously defines the existences of tri-dentate $L_{\bar{N}NO}$ (bridging) and bi-dentate L_{NNOH} (with the pendant phenol function) ligands in [5]Cl_2·2H_2O. Two $L_{\bar{N}NO}$ ligands are trans to each other and make approximately a Ni_2O_2 rectangle. Because of insufficient diffraction data, the structure of [5]Cl_2·2H_2O was not solved satisfactorily and the bond parameters of this complex was not reported.

3.3. Steady state fluorescence spectra in different solvents

On the contrary to the $[M(L_R^{\phi})X_2]$ complexes which are non-emissive in fluid solutions at 298 K, **1–3**, [4]Cl and [5]Cl_2

Table 3
Selected experimental bond lengths (Å) and angles (°) of [4]Cl·H_2O and calculated bond lengths (Å) and angles (°) of $[4]^+$.

	Exp.	Calc.		Exp.	Calc.
Co(1)–O(1)	1.887(2)	1.887	C(37)–N(38)	1.413(3)	1.392
Co(1)–O(31)	1.884(2)	1.887	N(38)–C(39)	1.302(3)	1.309
Co(1)–N(8)	1.884(2)	1.916	C(39)–C(40)	1.473(4)	1.471
Co(1)–N(15)	1.933(2)	1.970	C(39)–C(46)	1.491(4)	1.490
Co(1)–N(38)	1.888(2)	1.916	C(40)–N(45)	1.371(3)	1.363
Co(1)–N(45)	1.916(2)	1.970	O(1)–Co(1)–N(8)	87.33(9)	86.82
O(1)–C(2)	1.327(3)	1.314	N(8)–Co(1)–N(15)	83.72(10)	83.69
C(2)–C(7)	1.421(4)	1.433	N(150–Co(1)–N(38)	100.62(10)	99.57
C(7)–N(8)	1.408(3)	1.392	O(1)–Co(1)–N(38)	88.42(9)	89.88
N(8)–C(9)	1.303(3)	1.308	O(1)–Co(1)–O(31)	91.09(9)	91.49
C(9)–C(10)	1.469(4)	1.471	O(31)–Co(1)–N(38)	87.34(9)	86.81
C(9)–C(16)	1.487(4)	1.490	N(45)–Co(1)–N(38)	83.89(10)	83.72
C(10)–N(15)	1.367(3)	1.363	O(1)–Co(1)–N(15)	170.76(9)	170.54
O(31)–C(32)	1.325(3)	1.314	N(8)–Co(1)–N(38)	174.95(10)	175.26
C(32)–C(37)	1.416(3)	1.433	O(31)–Co(1)–N(45)	171.20(9)	170.52

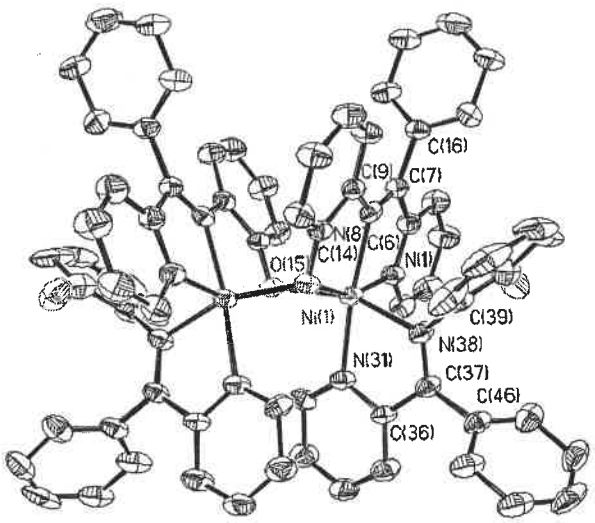

Fig. 4. Molecular geometry of $[5]^{2+}$ ion in crystals (50% thermal ellipsoids and hydrogen atoms are omitted for clarity).

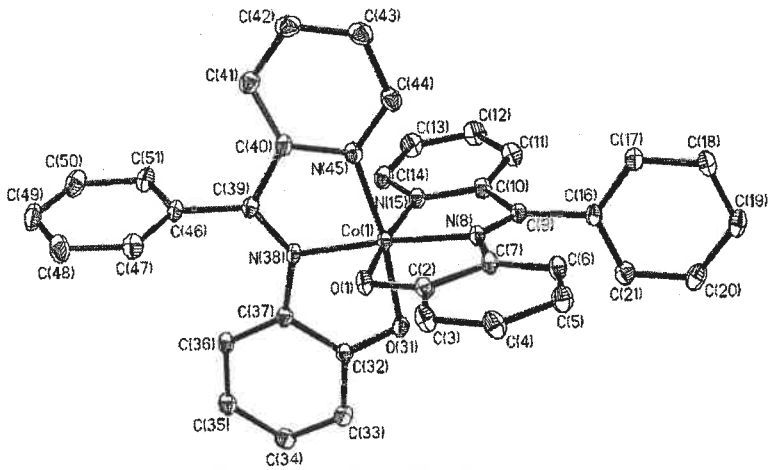

Fig. 3. Molecular geometry of $[4]^+$ ion in crystals (50% thermal ellipsoids and hydrogen atoms are omitted for clarity).

complexes are brightly fluorescent in fluid solutions due to restricted atropisomerism. The steady state emission spectra of all the complexes were recorded in CH_2Cl_2 and CH_3OH at 298 K and the emission and excitation spectra are shown in Figs. 5 and 6 and S2. The fluorescence spectral data are summarized in Table 4. It is noted that in CH_2Cl_2 the spectra of all the complexes are structured and well resolved. The excitation spectra correlate well to the corresponding UV–Vis absorption spectra of the complexes. Both the absorption and emission maxima of the complexes are blue shifted in CH_2Cl_2. The quantum yields in CH_2Cl_2 are comparatively higher. The quantum yield of **[4]Cl** is found to be maximum. The bromo and the cadmium analogues emit weakly. The origins of the excitation or absorption of the complexes were elucidated by TD DFT calculations on **1** and $[\mathbf{4}]^+$ (*vide infra*).

3.4. Time resolved emission spectra

The fluorescence lifetimes of **1–3**, **[4]Cl** and $[\mathbf{5}]Cl_2$ were measured using λ_{ex} = 470 nm in CH_2Cl_2 and MeOH at 298 K monitoring the λ_{max} of the corresponding emission spectra. The lifetime data are summarized in Table 5. The decay of the emissions of the complexes **1–3** in CH_2Cl_2 are shown in Fig. S3. The fluorescence decay in all cases was found to fit with two components with χ^2 value ≈1. Two component lifetimes originate may be due to the conjugated and non-conjugated orientations of the pendent phenyl ring to the 14πe of the coordinated $L_{\widetilde{NNO}}$ ligand (Chart 2). The values of the lifetimes with their percentage contribution along with the corresponding χ^2 values and τ_{av} are listed in Table 5. The percentage contributions of the longer components decreases from **1** to **3**, while the trend is reverse for shorter components. The average lifetime values corroborate well with the respective quantum yield data. **3** exhibits shorter average lifetime with the larger amplitude of the lower component resulting in a lower fluorescence quantum yield compared to the other complexes. This could be due to higher spin orbit coupling in cadmium. The fluorescence quantum yield of **[4]Cl** is maximum having maximum fluorescence lifetime and in case of $[\mathbf{5}]Cl_2$ these values are minimum (Table 5).

Table 4
Fluorescence data of the **1–3**, **[4]Cl** and $[\mathbf{5}]Cl_2$ in CH_2Cl_2 and MeOH solutions at 298 K.

Complexes	Solvent	λ_{ex} (nm)	λ_{em} (nm)
1	MeOH	505	555
	CH_2Cl_2	475, 507	520, 551
2	MeOH	505	557
	CH_2Cl_2	474, 507	519, 552
3	MeOH	505	560
	CH_2Cl_2	474, 507	518, 551
[4]Cl	MeOH	472, 500	568
	CH_2Cl_2	472, 505	518, 551, 601
$[\mathbf{5}]Cl_2$	MeOH	470, 510	580
	CH_2Cl_2	472, 506	520, 557, 595

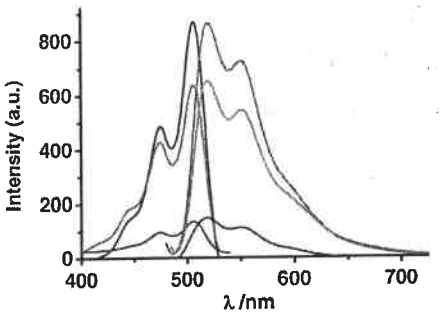

Fig. 5. Excitation and emission spectra of **1–3** in CH_2Cl_2 at 298 K: excitation (black) and emission (cyan) spectra of **1**; excitation (red) and emission (pink) spectra of **2**; excitation (blue) and emission (wine) spectra of **3**. (For interpretation of the references to color in this figure legend, the reader is referred to the web version of this article).

3.5. Density functional theory (DFT) and time dependent (TD) DFT calculations

The ground state electronic structure of $[\mathbf{5}]^{2+}$ cation and the photoactive orbitals of **1** and $[\mathbf{4}]^+$ ion were elucidated by DFT and TD DFT calculations. The gas phase geometries of **1** and $[\mathbf{4}]^+$ were optimized with singlet spin state using restricted B3LYP functional, while the gas phase geometry of $[\mathbf{5}]^{2+}$ ion was optimized with quintet spin state. The optimized geometries are depicted in Figs. 7 and 8 and S4. The calculated bond parameters of **1** are listed under the caption of Fig. 7 while the optimized bond parameters of $[\mathbf{4}]^+$ and $[\mathbf{5}]^{2+}$ ions are summarized in Tables 3 and S1 respectively. The calculated bond parameters are comparable to those obtained from the single crystal X-ray structure determinations of $[\mathbf{4}]Cl{\cdot}H_2O$.

The Mulliken spin density plot of $[\mathbf{5}]^{2+}$ cation is depicted in Fig. 8. Atomic spin densities are listed under the Figure caption. Analyses of Mulliken atomic spin densities affirm that the spin densities are localized on the metal centers confirming the existence of two nickel(II) ion in the $[\mathbf{5}]^{2+}$ cation. It correlates well with the magnetic moment features of $[\mathbf{5}]Cl_2$. No significant distribution of the spin density over the diimine ligand is noted.

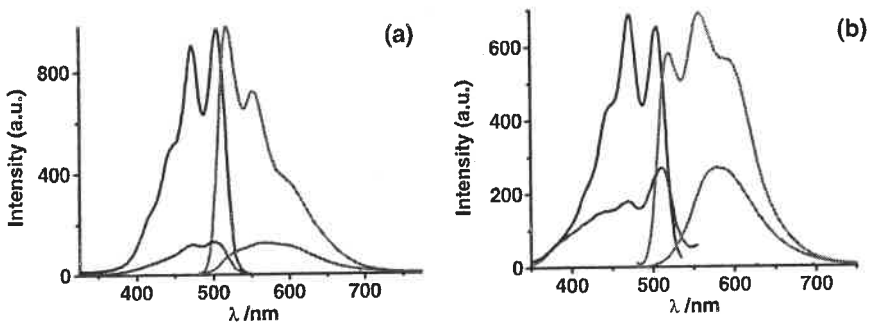

Fig. 6. (a) Excitation (blue) and emission (cyan) in MeOH and excitation (black) and emission (red) in CH_2Cl_2 of **[4]Cl**. (b) Excitation (blue) and emission (cyan) in MeOH and excitation (black) and emission (red) in CH_2Cl_2 of $[\mathbf{5}]Cl_2$. (For interpretation of the references to color in this figure legend, the reader is referred to the web version of this article).

Table 5
Fluorescence lifetime data of **1–3**, [4]Cl and [5]Cl_2 in CH_2Cl_2 and MeOH at 298 K.

Comp.	Solvents	λ_{ex} (nm)	$\lambda_{monitored}$ (nm)	Φ	Singlet state lifetime monitoring the respective emission maxima			
					τ_1 (ns)	τ_2 (ns)	χ^2	$\langle\tau\rangle$ (ns)
1	CH_2Cl_2	470	520	0.037	3.7(42.54%)	1.7(57.44%)	1.09	2.6
	CH_3OH	470	540	0.003	2.7(27.38%)	1.2(72.62%)	1.14	1.6
2	CH_2Cl_2	470	520	0.027	3.6(39.78%)	1.6(60.22%)	1.19	2.4
	CH_3OH	470	540	0.002	2.8(23.55%)	1.2(76.45%)	0.92	1.6
3	CH_2Cl_2	470	520	0.010	3.8(24.95%)	0.7(75.05%)	0.91	2.0
	CH_3OH	470	532	0.0007	2.7(18.27%)	1.2 (81.73%)	1.22	1.4
[4]Cl	CH_2Cl_2	470	520	0.060	6.6 (52.81%)	0.9(47.20%)	0.92	3.9
	CH_3OH	470	532	0.040	4.1(25.56%)	1.1(74.44%)	0.90	1.8
[5]Cl_2	CH_2Cl_2	470	520	0.002	2.5(66.62%)	0.6(33.38%)	1.18	1.9
	CH_3OH	470	555	0.0002	1.8(82.93%)	0.5(17.10%)	0.97	1.6

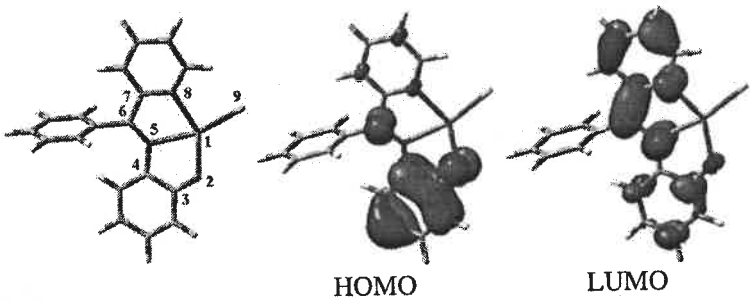

Fig. 7. Optimized geometry and photoactive orbitals of **1** (Zn1–O2 1.999; Zn1–N5 2.208; Zn1–N8 2.303; Zn1–Cl9 2.263; O2–C3 1.296; C4–N5 1.380; N5–C6 1.295; C6–C7 1.484 Å).

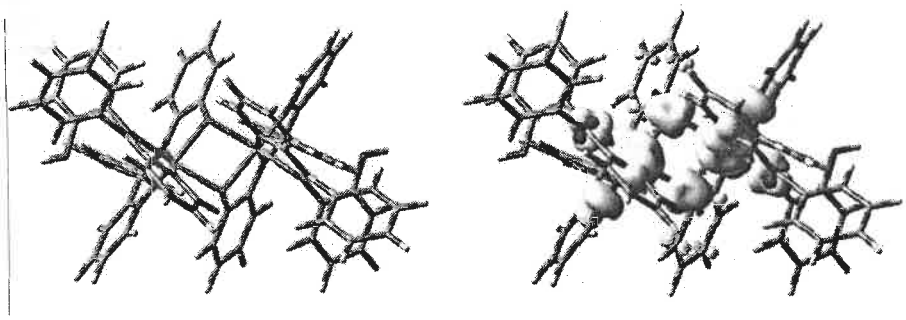

Fig. 8. Optimized geometry and Mulliken spin density plot of $[5]^{2+}$ cation. [Spin density of a NiN_4O_2 octahedron of $[5]^{2+}$: Ni 1.63, N(1) 0.06, N(8) 0.08, N(31) 0.05, N(38) 0.06, O(15) 0.10].

The photoactive orbitals of **1** and $[4]^+$ cation were authenticated by TD DFT calculations. Excitation energies (λ/nm), oscillator strengths (f), transition types and dominant contributions of the excitation bands of **1** and $[4]^+$ cation are listed in Table 6. TD DFT calculations on **1** and $[4]^+$ cation were performed in CH_2Cl_2 using CPCM model. The calculated spectra of **1** and $[4]^+$ are illustrated in Fig. S5. The calculations revealed that the lowest energy absorption at 509 nm of **1** is due to the transitions from the HOMO to LUMO, which are localized respectively on $\pi_{phenolato}$ and $\pi^*_{diimine}$ molecular orbitals as shown in Fig. 7. It infers that **1–3** complexes are fluorescent due to the intra-ligand $\pi_{phenolato} \rightarrow \pi^*_{diimine}$ transition.

On the contrary, it is observed that the photo active $\pi_{phenolato}$ and $\pi^*_{diimine}$ orbitals of brightly fluorescent $[4]^+$ are delocalized over the two L_{NNO}^- ligands. The responsible photoactive HOMO and LUMO orbitals of $[4]^+$ are illustrated in Fig. 9. The structures of the photo active orbitals are similar to those obtained in the $[M(L_R^{\phi})X_2]$ complexes due to π–π stacking attributing $\pi_{diimine}$ and $\pi^*_{diimine}$ delocalization over the layers making complexes fluorescent in solid state [2a]. However in case of $[4]^+$ ion $\pi_{phenolato}$ and $\pi^*_{diimine}$ orbitals delocalization occurs even in solution. TD DFT calculation on $[4]^+$ established that the lower energy excitations at 541 and 536 nm are due to the inter-ligand $\pi_{phenolato}$ (HOMO-1) $\rightarrow$ $\pi^*_{diimine}$ (LUMO + 1) and $\pi_{phenolato}$ (HOMO) $\rightarrow$ $\pi^*_{diimine}$ (LUMO + 1) transitions. HOMO and HOMO-1 are constituted of the phenolato rings and are more stabilized in polar solvents, while LUMO and LUMO + 1 are delocalized over $\pi^*_{diimine}$ orbitals. Thus **1–3** are fluorescent due to the intra-ligand charge transfer (ILCT) within the 14πe diimine fragment while the [4]Cl exhibits transitions among the delocalized $\pi_{phenolato}$ and $\pi^*_{diimine}$ orbitals resulting in a maximum fluorescence quantum yield for [4]Cl.

Table 6
Excitation energies (λ/nm), oscillator strengths (f), transition types and dominant contributions of UV–Vis absorption bands of **1** and **[4]**$^{+}$ obtained from TD DFT calculations.

λ_{cal}	f	λ_{exp}	Significant transitions (>15%)	Dominant contributions
1				
509	0.297	507	H → L (86)	L1(99) → L1(98)
		475		
		447		
355	0.26	355	H-1 → L (83)	L1(100) → L1(98)
340	0.117		H → L + 1 (89)	L1(99) → L1(100)
315	0.042		H-3 → L (82)	Cl(95) → L1(98)
[4]$^{+}$				
541	0.141		H-1 → L + 1 (20)	L1(90) → L1(49) + L2(48)
			H → L + 1 (41)	L2(89) → L1(49) + L2(48)
536	0.2		H-1 → L + 1 (37)	L1(90) → L1(49) + L2(48)
			H → L (16)	L2(89) → L1(48) + L2(49)
			H → L + 1 (18)	L2(89) → L1(49) + L2(48)
472	0.02	448	H-1 → L + 2 (33)	L1(90) → Co(60) + L1(21)
			H → L + 2 (52)	L2(89) → Co(60) + L1(21)
373	0.131		H-2 → L (68)	L1(41) + L2(59) → L1(48) + L2(49)
371	0.121		H-3 → L (83)	L1(59) + L2(41) → L1(48) + L2(49)
368	0.037		H-2 → L + 1 (85)	L1(41) + L2(59) → L1(49) + L2(48)
365	0.079		H-3 → L + 1 (85)	L1(59) + L2(41) → L1(49) + L2(48)
350	0.035	353	H-7 → L (22)	L1(41) + L2(58) → L1(48) + L2(49)
			H-4 → L + 1(17)	L1(53) + L2(46) → L1(49) + L2(48)

L1 = L2 = $L_{\bar{N}NO}$ H = HOMO, L = LUMO.

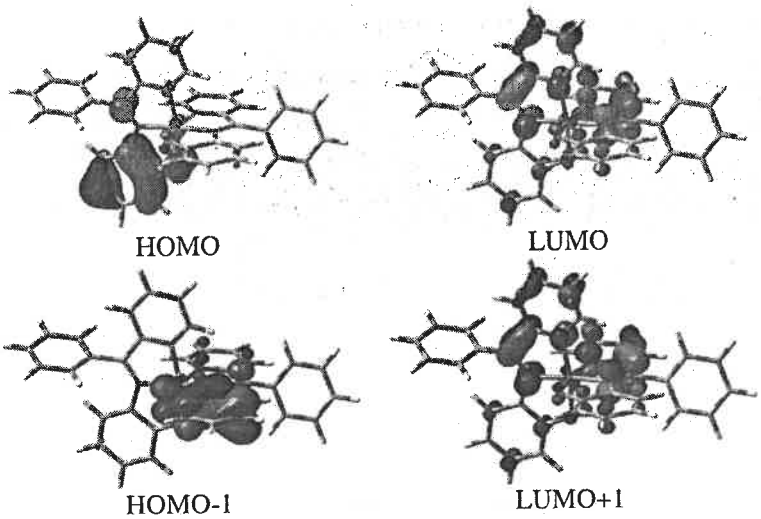

Fig. 9. Photoactive orbitals of **[4]**$^{+}$.

4. Conclusions

Recently, structural and spectral analyses of atropisomeric unsymmetrical diimine (L_R^{ϕ}) complexes [2a] of type [M(L_R^{ϕ})X_2], (Type-I) (M = Zn, Cd; X = Cl, Br; R = Me, CMe_3, OH, OMe, Cl), [(L_{Me2}^{ϕ})$ZnBr_2$] (Type-II), (L_{OH}^{ϕ})$PdCl_2$ (Type-III) established that the photoluminescence of these complexes depend on the atropisomerism of the L_R^{ϕ} ligand and π–π stacking (ϕ = dihedral angle between the diimine unit including the pyridine ring and the phenyl ring planes). Type-I isomers in crystals display π–π stacking with $\phi = 0°$ and behave like a conjugated aromatics with 14π electrons (14πe) system, π iso-electronic with anthracene and likewise strongly fluorescent in solid state. In solutions, in absence of π–π stacking and planarity of ligand, Type-I isomers are non-emissive but frozen glasses of these complexes at 77 K are emissive displaying blue shifted structured spectra. While the atropisomers with $\phi = 90°$ (Type-II complexes) are ineligible to attain planarity *via* π–π stacking and are non-emissive in solid state and solutions.

The present work in conjunction with a recent report [2b] supports the above analogy that the coordination complexes of the diimine ligand with conjugated 14πe are emissive alike anthracene. In this work, spectral and structural features of the three types of complexes of a tri-dentate diimine ligand [L_{NNOH} = (*E*)-2-((phenyl(pyridin-2-yl)methylene)amino)phenol] incorporating 14πe with zinc(II), cadmium(II), cobalt(III) and nickel(II) ions are authenticated. The complexes are mononuclear complexes of type [M($L_{\bar{N}NO}$)X] [M = Zn, X = Cl, **1**; M = Zn, X = Br, **2**; M = Cd, X = Cl, **3**], mononuclear bis L_{NNOH} complex of type, [Co($L_{\bar{N}NO}$)$_2$]Cl, **[4]**Cl and unusual dinuclear μ-L_{NNOH} complex of type [Ni_2(L_{NNOH})$_2$($L_{\bar{N}NO}$)$_2$]Cl_2, **[5]**Cl_2. In all cases the L_{NNOH} ligand orients with $\phi = 0$. Unlike

$[M(L_R^{\phi})X_2]$, complexes, **1–3**, **[4]**Cl and **[5]**Cl_2 are fluorescent in fluid solutions at 298 K. DFT calculations disclosed that $\pi_{phenolato} \rightarrow \pi^*_{diimine}$ (intra- or both intra- and inter-ligand) transitions are the origins of the emissive excitation of the complexes. The work infers that diimine complexes with conjugated 14πe are fluorescent due to $\pi \rightarrow \pi^*$ transitions.

Acknowledgments

Financial support received from DST (SR/S1/IC/0026/2012) and CSIR (01/2699/12/EMR-II), New Delhi, India is gratefully acknowledged. S.K. is thankful to CSIR, New Delhi, India, for SRF fellowships.

Appendix A. Supplementary material

CCDC 943148 and 943149 contain the supplementary crystallographic data for complexes **[4]**Cl·H_2O and **[5]**Cl_2·$2H_2O$ respectively. These data can be obtained free of charge from The Cambridge Crystallographic Data Centre via www.ccdc.cam.ac.uk/data_request/cif, electronic spectra of **1–3**, **[4]**Cl and **[5]**Cl_2 in CH_3OH (Fig. S1), excitation and emission spectra of **1–3** in CH_3OH (Fig. S2), fluorescence decay of complex **1–3** in CH_2Cl_2 (Fig. S3), optimized gas phase geometry of **[4]**$^+$ (Fig. S4), calculated bond parameters of **[5]**$^{2+}$ (Table S1), electronic absorption spectra of **1** and **[4]**$^+$ obtained from TD DFT calculations (Fig. S5) and gas phase optimized coordinates of **1**, **[4]**$^+$ and **[5]**$^{2+}$ using B3LYP functionals (Tables S2–S5). Supplementary data associated with this article can be found, in the online version, at http://dx.doi.org/10.1016/j.ica.2015.02.032.

References

[1] (a) K. Hasan, L. Donato, Y. Shen, J.D. Slinker, E. Zysman-Colman, Dalton Trans. 43 (2014) 13672;
(b) S. Evariste, M. Sandroni, T.W. Rees, C. Roldán-Carmona, L. Gil-Escrig, H.J. Bolink, E. Baranoff, E. Zysman-Colman, J. Mater. Chem. C 2 (2014) 5793;
(c) Z. Ye, X. An, B. Song, W. Zhang, Z. Dai, J. Yuan, Dalton Trans. 43 (2014) 13055;
(d) Z. Ye, R. Zhang, B. Song, Z. Dai, D. Jin, E.M. Goldys, J. Yuan, Dalton Trans. 43 (2014) 8414;
(e) S. Ray, S. Konar, A. Jana, K. Das, A. Dhara, S. Chatterjee, S.K. Kar, J. Mol. Struct. 1058 (2014) 213;
(f) A. Jana, P.K. Sukul, S.K. Mandal, S. Konar, S. Ray, K. Das, J.A. Golen, A.L. Rheingold, S. Mondal, T.K. Mondal, A.R.K. Bukhsh, S.K. Kar, Analyst 139 (2014) 495;
(g) Z. Ye, B. Song, Y. Yin, R. Zhang, J. Yuan, Dalton Trans. 42 (2013) 14380;
(h) H. Xiang, J. Cheng, X. Ma, X. Zhou, J.J. Chruma, Chem. Soc. Rev. 42 (2013) 6128;
(i) W.-K. Chung, K.M.-C. Wong, W.H. Lam, X. Zhu, N. Zhu, H.-S. Kwok, V.W.-W. Yam, New J. Chem. 37 (2013) 1753;
(j) R. Liu, N. Dandu, Y. Li, S. Kilina, W. Sun, Dalton Trans. 42 (2013) 4398;
(k) R. Liu, H. Chen, J. Chang, Y. Li, H. Zhu, W. Sun, Dalton Trans. 42 (2013) 160;
(l) Z. Li, W. Sun, Dalton Trans. 42 (2013) 14021;
(m) Z. Li, E. Badaeva, A. Ugrinov, S. Kilina, W. Sun, Inorg. Chem. 52 (2013) 7578;
(n) R. Liu, A. Azenkeng, D. Zhou, Y. Li, K.D. Glusac, W. Sun, J. Phys. Chem. A 117 (2013) 1907;
(o) T. Lazarides, T.M. McCormick, K.C. Wilson, S. Lee, D.W. McCamant, R. Eisenberg, J. Am. Chem. Soc. 133 (2011) 350;
(p) K.K. Sadhu, S. Sen, P.K. Bharadwaj, Dalton Trans. 40 (2011) 726;
(q) M.D. Ward, Coord. Chem. Rev. 254 (2010) 2634;
(r) T.L. Easun, W.Z. Alsindi, N. Deppermann, M. Towrie, K.L. Ronayne, X.-Z. Sun, M.D. Ward, M.W. George, Inorg. Chem. 48 (2009) 8759;
(s) T. Lazarides, M.A.H. Alamiry, H. Adams, S.J.A. Pope, S. Faulkner, J.A. Weinstein, M.D. Ward, Dalton Trans. (2007) 1484;
(t) V.W.-W. Yam, (Ed.) Photofunctional Transition Metal Complexes: Springer: Series: Structure and Bonding, Vol. 123, 2007.:
(u) M.J. Li, B.W.K. Chu, N. Zhu, V.W.-W. Yam, Inorg. Chem. 46 (2007) 720;
(v) M.D. Ward, Coord. Chem. Rev. 251 (2007) 1663;
(w) C. Yu, K.M.C. Wong, K.H.Y. Chan, V.W.-W. Yam, Angew. Chem., Int. Ed. 44 (2005) 791;
(x) M. Hissler, J.E. McGarrah, W.B. Connick, D.K. Geiger, S.D. Cummings, R. Eisenberg, Coord. Chem. Rev. 208 (2000) 115.

[2] (a) A.S. Roy, P. Saha, P. Mitra, S.S. Maity, S. Ghosh, P. Ghosh, Dalton Trans. 40 (2011) 7375;
(b) S. Kundu, S. Maity, P.S. Sardar, S. Ghosh, P. Ghosh, Dalton Trans. 42 (2013) 13026.

[3] (a) G.M. Sheldrick, SHELXS97, Universität Göttingen, Göttingen, Germany, 1997;
(b) G.M. Sheldrick, SHELXL97, Universität Göttingen, Göttingen, Germany, 1997.

[4] M.J. Frisch, G.W. Trucks, H.B. Schlegel, G.E. Scuseria, M.A. Robb, J.R. Cheeseman Jr., J.A. Montgomery, T. Vreven, K.N. Kudin, J.C. Burant, J.M. Millam, S.S. Iyengar, J. Tomasi, V. Barone, B. Mennucci, M. Cossi, G. Scalmani, N. Rega, G.A. Petersson, H. Nakatsuji, M. Hada, M. Ehara, K. Toyota, R. Fukuda, J. Hasegawa, M. Ishida, T. Nakajima, Y. Honda, O. Kitao, H. Nakai, M. Klene, X. Li, J.E. Knox, H.P. Hratchian, J.B. Cross, V. Bakken, C. Adamo, J. Jaramillo, R. Gomperts, R.E. Stratmann, O. Yazyev, A.J. Austin, R. Cammi, C. Pomelli, J.W. Ochterski, P.Y. Ayala, K. Morokuma, G.A. Voth, P. Salvador, J.J. Dannenberg, V.G. Zakrzewski, S. Dapprich, A.D. Daniels, M.C. Strain, O. Farkas, D.K. Malick, A.D. Rabuck, K. Raghavachari, J.B. Foresman, J.V. Ortiz, Q. Cui, A.G. Baboul, S. Clifford, J. Cioslowski, B.B. Stefanov, G. Liu, A. Liashenko, P. Piskorz, I. Komaromi, R.L. Martin, D.J. Fox, T. Keith, M.A. Al-Laham, C.Y. Peng, A. Nanayakkara, M. Challacombe, P.M.W. Gill, B. Johnson, W. Chen, M.W. Wong, C. Gonzalez, J.A. Pople, GAUSSIAN 03, revision E.01, Gaussian Inc., Wallingford, CT, 2004.

[5] (a) R.G. Parr, W. Yang, Density Functional Theory of atoms and molecules. Oxford University Press, Oxford, UK, 1989;
(b) D.R. Salahub, M.C. Zerner, The Challenge of d and f Electrons: ACS Symposium Series 394, American Chemical Society, Washington, DC, 1989;
(c) W. Kohn, L. Sham, J. Phys. Rev. 104 (1965) A1133;
(d) P. Hohenberg, W. Kohn, Phys. Rev. 136 (1964) B864.

[6] (a) R.E. Stratmann, G.E. Scuseria, M. Frisch, J. Chem. Phys. 109 (1998) 8218;
(b) M.E. Casida, C. Jamoroski, K.C. Casida, D.R. Salahub, J. Chem. Phys. 108 (1998) 4439;
(c) R. Bauernschmitt, M. Haser, O. Treutler, R. Ahlrichs, Chem. Phys. Lett. 256 (1996) 454.

[7] (a) A.D. Becke, J. Chem. Phys. 98 (1993) 5648;
(b) B. Miehlich, A. Savin, H. Stoll, H. Preuss, Chem. Phys. Lett. 157 (1989) 200;
(c) C. Lee, W. Yang, R.G. Parr, Phys. Rev. B 37 (1988) 785.

[8] P.J. Pulay, Comput. Chem. 3 (1982) 556.

[9] H.B. Schlegel, J.J. McDouall, in: C. Ogretir, I.G. Csizmadia (Eds.), Computational Advances in Organic Chemistry, Kluwer Academic, The Netherlands, 1991, pp. 167–185.

[10] (a) P.J. Hay, W.R. Wadt, J. Chem. Phys. 82 (1985) 270;
(b) W.R. Wadt, P.J. Hay, J. Chem. Phys. 82 (1985) 284;
(c) P.J. Hay, W.R. Wadt, J. Chem. Phys. 82 (1985) 299.

[11] (a) V.A. Rassolov, M.A. Ratner, J.A. Pople, P.C. Redfern, L.A. Curtiss, J. Comput. Chem. 22 (2001) 976;
(b) M.M. Francl, W.J. Pietro, W.J. Hehre, J.S. Binkley, D.J. DeFrees, J.A. Pople, M.S. Gordon, J. Chem. Phys. 77 (1982) 3654;
(c) P.C. Hariharan, J.A. Pople, Mol. Phys. 27 (1974) 209;
(d) P.C. Hariharan, J.A. Pople, Theor. Chim. Acta. 28 (1973) 213;
(e) W.J. Hehre, R. Ditchfield, J.A. Pople, J. Chem. Phys. 56 (1972) 2257.

[12] (a) G.A. Petersson, M.A. Al-Laham, J. Chem. Phys. 94 (1991) 6081;
(b) G.A. Petersson, A. Bennett, T.G. Tensfeldt, M.A. Al-Laham, W.A. Shirley, J. Mantzaris, J. Chem. Phys. 89 (1988) 2193.

[13] N.M. O'Boyle, A.L. Tenderholt, K.M. Langner, J. Comput. Chem. 29 (2008) 839.

[14] (a) M. Cossi, N. Rega, G. Scalmani, V. Barone, J. Comput. Chem. 24 (2003) 669;
(b) V. Barone, M. Cossi, J. Phys. Chem. A 102 (1998) 1995.

[15] (a) A.T.R. Williams, S.A. Winfield, J.N. Miller, Analyst 108 (1983) 1067;
(b) J.R. Lakowicz (Ed.), Principles of Fluorescence Spectroscopy, second ed., Kluwer Academic/Plenum Publishers, NY, 2003.

[16] FELIX 32, Operation Manual, Version 1.1, Photon Technology International Inc., NJ, 2003.